



## Chemical looping combustion of biomass using metal ferrites as oxygen carriers



Xun Wang<sup>a</sup>, Zhihua Chen<sup>b</sup>, Mian Hu<sup>a</sup>, Yufei Tian<sup>c</sup>, Xiaoyu Jin<sup>a</sup>, Shu Ma<sup>a</sup>, Tingting Xu<sup>a</sup>, Zhiquan Hu<sup>a</sup>, Shiming Liu<sup>a</sup>, Dabin Guo<sup>a</sup>, Bo Xiao<sup>a,\*</sup>

<sup>a</sup>School of Environmental Science & Engineering, Huazhong University of Science & Technology, Wuhan 430074, China

<sup>b</sup>School of Environment, Henan Normal University, No. 46, Jianshe Road, Xinxiang 453007, Henan, China

<sup>c</sup>School of Energy and Power Engineering, Huazhong University of Science & Technology, Wuhan 430074, China

### HIGHLIGHTS

- CuFe<sub>2</sub>O<sub>4</sub> has the highest reactivity and a lower initial reaction temperature in biomass CLC.
- NiFe<sub>2</sub>O<sub>4</sub> has the highest catalytic reactivity for tar cracking and reforming.
- CoFe<sub>2</sub>O<sub>4</sub> is easily reduced to FeO and three metal ferrites can be regenerated completely after five redox cycles.
- Both CuFe<sub>2</sub>O<sub>4</sub> and CoFe<sub>2</sub>O<sub>4</sub> have remarkable thermal stability.
- The reactivity of NiFe<sub>2</sub>O<sub>4</sub> decreases significantly after five redox cycles due to sintering.

### ARTICLE INFO

#### Article history:

Received 3 October 2016

Received in revised form 23 November 2016

Accepted 24 November 2016

Available online 25 November 2016

#### Keywords:

Chemical looping combustion

Metal ferrites

CO<sub>2</sub> capture

Pine sawdust

### ABSTRACT

The evaluation of chemical looping combustion (CLC) for CO<sub>2</sub> capture was conducted via a thermogravimetric analyzer (TGA) and a laboratory-scale fluidized bed using pine sawdust (PS) as fuel and metal ferrites, MFe<sub>2</sub>O<sub>4</sub> (M = Cu, Ni and Co), as oxygen carriers. Metal ferrites were prepared by sol-gel method. The fresh, reduced and after five redox cycles oxygen carriers were characterized by X-ray diffraction (XRD), scanning electron microscopy (SEM) and accelerated surface area porosimetry. Thermodynamic simulation was performed using software HSC Chemistry 6.0. The TGA results indicated that CuFe<sub>2</sub>O<sub>4</sub> shows a lower initial reaction temperature, and CoFe<sub>2</sub>O<sub>4</sub> has a faster oxygen uptake rate. Both carbon conversion ( $\alpha_c$ ) and carbon capture efficiency ( $\eta_{CO_2}$ ) increased with temperature. The maximum values of  $\alpha_c$  and  $\eta_{CO_2}$  were 96.86% and 95.48%, 95.45% and 94.25%, and 95.17% and 94.04% for CuFe<sub>2</sub>O<sub>4</sub>, CoFe<sub>2</sub>O<sub>4</sub>, and NiFe<sub>2</sub>O<sub>4</sub> at 900 °C, respectively. The CuFe<sub>2</sub>O<sub>4</sub> shows higher reaction reactivity, while NiFe<sub>2</sub>O<sub>4</sub> has a higher catalytic activity for decomposition of tar in fluidized bed tests. The XRD results show CoFe<sub>2</sub>O<sub>4</sub> is more readily reduced to FeO, which agreed with the results of thermodynamic simulation, and three metal ferrites can be regenerated completely after five cycles. The values of  $\alpha_c$  and  $\eta_{CO_2}$  remained high for both CuFe<sub>2</sub>O<sub>4</sub> and CoFe<sub>2</sub>O<sub>4</sub>, while a significant decrease in  $\alpha_c$  and  $\eta_{CO_2}$  for NiFe<sub>2</sub>O<sub>4</sub> was observed after five cycles due to significant sintering. Both CuFe<sub>2</sub>O<sub>4</sub> and CoFe<sub>2</sub>O<sub>4</sub> are more applicable as oxygen carriers in biomass CLC compared with NiFe<sub>2</sub>O<sub>4</sub>.

© 2016 Elsevier B.V. All rights reserved.

## 1. Introduction

The concerns of global warming and climate change have resulted in efforts to reduce carbon dioxide (CO<sub>2</sub>) emissions by adopting carbon capture and storage (CCS) technologies or increasing the utilization of renewable energies [1]. The purpose of CCS technologies is to capture and store pure streams of CO<sub>2</sub> from

the atmosphere [2]. Currently, in order to capture CO<sub>2</sub>, there are three main approaches: post-combustion, oxy-fuel combustion, and pre-combustion [3]. Although these methods can reduce the CO<sub>2</sub> emissions effectively, they typically involve large-scale gas separations, which require significant energy and economic investments. The chemical looping combustion (CLC) has been considered a promising technology for low-cost CO<sub>2</sub> emissions reduction [4]. In general, the CLC process consists of an air reactor (AR) and a fuel reactor (FR). An oxygen carrier is utilized to transfer

\* Corresponding author.

E-mail address: [xiaobo1958@hust.edu.cn](mailto:xiaobo1958@hust.edu.cn) (B. Xiao).

oxygen from AR to FR. Thus, the CLC process does not require a gas separation unit because the air and fuel are never mixed.

In recent years, a lot of work has been done concerning CLC with gaseous fuels [5–7]. More recently, CLC has shown great potential for better utilizing solid fuels, such as coal [8], petroleum coke [9], sewage sludge [10], and biomass [11], because of abundant solid fuel resources.

As a renewable and carbon neutral resource, biomass is expected to significantly contribute to global energy and environmental demands [12]. What is noteworthy is that carbon emissions in CLC will be negative when replacing fossil fuels with biomass because the generated CO<sub>2</sub> is previously absorbed by photosynthesis. Furthermore, biomass CLC has additional advantages, such as higher carbon conversion efficiency [13,14] as well as lower NO<sub>x</sub> [15] and SO<sub>2</sub> emissions [16].

Oxygen carrier is the backbone of the CLC process. Ideally, the oxygen carrier should have high transport capacity, reactivity, and thermal stability, with low production costs and no environmental impacts [17]. Transition single metal oxides, such as Cu, Ni, Co, Mn and Fe, have been widely investigated in CLC despite some disadvantages and inability to fully meet the requirements of CLC. More specifically, CuO readily agglomerates due to its lower melting point; NiO and CoO have adverse environmental effects and are expensive; and MnO and Fe<sub>2</sub>O<sub>3</sub> have poor oxygen transfer capacity and low reactivity. In order to find a perfect oxygen carrier, an increasing number of studies have focused on combined or mixed-metal oxides. For example, Fe<sub>2</sub>O<sub>3</sub> has been widely used in combined or mixed-metal oxide oxygen carrier systems due to its low cost, environmental friendliness and abundance. Metal ferrites, MFe<sub>2</sub>O<sub>4</sub>, yielded favorable results in CLC when using combined or mixed Fe<sub>2</sub>O<sub>3</sub> and another metal oxide as oxygen carrier.

Niu et al. [18] studied Cu-Fe oxygen carrier for CLC using sewage sludge as fuel. They found that the presence of CuFe<sub>2</sub>O<sub>4</sub> enhanced the performance of Fe<sub>2</sub>O<sub>3</sub> and improved the thermal stability of CuO. Similar results were published by Wang et al. [19]. Bhavsar et al. [20] investigated the performance of bimetallic oxygen carriers in thermogravimetric analyzer (TGA) and a fixed-reactor using H<sub>2</sub> and CH<sub>4</sub> as fuels. They concluded that the reactivity of NiFe<sub>2</sub>O<sub>4</sub> was higher than Fe<sub>2</sub>O<sub>3</sub> but lower than NiO. Kuo et al. [21] also confirmed that NiFe<sub>2</sub>O<sub>4</sub> withstood higher cycle numbers and had greater stability than those of NiO and Fe<sub>2</sub>O<sub>3</sub> using CH<sub>4</sub> as fuel. The research results of Huang et al. [22] showed that the presence of NiFe<sub>2</sub>O<sub>4</sub> improved the reaction reactivity of the oxygen carrier with biochar. Wang et al. [23] indicated that CoFe<sub>2</sub>O<sub>4</sub> exhibited higher reactivity than CoO and Fe<sub>2</sub>O<sub>3</sub> in TGA using coal as fuel. Evdou et al. [24] demonstrated that CuFe<sub>2</sub>O<sub>4</sub> showed high reactivity towards CH<sub>4</sub> while CoFe<sub>2</sub>O<sub>4</sub> exhibited excellent thermal stability.

In general, metal ferrites with a spinel structure have high thermal stability and magnetic properties [25]. High thermal stability is favored as it increases the lifetime of the oxygen carrier, while magnetic properties of spinel metal ferrites could allow for the separation of the oxygen carrier from ash via magnetic separation technique. Therefore, metal ferrites exhibit great potential as oxygen carriers in solid CLC. To date, metal ferrites have been predominantly used as catalysts [26–29], and to authors' knowledge, the utilization of metal ferrites in biomass CLC remains few.

In this study, three metal ferrites, MFe<sub>2</sub>O<sub>4</sub> (M = Cu, Ni and Co), were evaluated in CLC using pine sawdust (PS) as fuel. TGA was used to analyze the reaction reactivity of PS with MFe<sub>2</sub>O<sub>4</sub>. The effects of temperature on carbon conversion ( $x_c$ ), CO<sub>2</sub> capture efficiency ( $\eta_{CO_2}$ ) and tar yield were measured in fluidized bed reactor. Thermodynamic simulation was performed to elucidate the conversion of MFe<sub>2</sub>O<sub>4</sub> (M = Cu, Ni and Co) during reduction reaction. The metal ferrites were investigated by a series of characterization techniques including XRD, SEM and BET. Finally, cyclic

performances of the metal ferrites were also evaluated via five redox cycle tests.

## 2. Methods

### 2.1. Materials

Raw pine sawdust (PS) was collected from a wood factory in Bijie City, Guizhou Province, China. The pine sawdust was naturally dried for seven days, then crushed and sieved to 75–250  $\mu$ m for use. The ultimate and proximate analysis of PS are given in Table 1.

### 2.2. Synthesis of oxygen carrier

Three metal ferrites, MFe<sub>2</sub>O<sub>4</sub> (M = Cu, Ni and Co), were prepared by the sol-gel combustion method [30]. First, stoichiometric amounts of Fe(NO<sub>3</sub>)<sub>3</sub>·9H<sub>2</sub>O, Cu(NO<sub>3</sub>)<sub>2</sub>·3H<sub>2</sub>O, Ni(NO<sub>3</sub>)<sub>2</sub>·6H<sub>2</sub>O, Co(NO<sub>3</sub>)<sub>2</sub>·6H<sub>2</sub>O and C<sub>6</sub>H<sub>8</sub>O<sub>7</sub>·H<sub>2</sub>O (citric acid) were dissolved in deionized water. Metal nitrates and the citric acid solution were mixed at a 1:1 M ratio of total metal cation (Fe<sup>3+</sup> and M<sup>2+</sup>) to citric acid. The citric acid was used as a chelating/fuel agent. Next, the precursor mixture solution was slowly stirred at 80 °C for 6 h, and the sol-gel was obtained. After that, the sol-gel was dried in a dryer at 105 °C for 12 h and ignited in the preheated muffle furnace at 650 °C for 10 min, followed by calcination at 900 °C for 6 h in air. Finally, metal ferrites samples were cooled, ground, and sieved to 75–250  $\mu$ m for use.

### 2.3. Thermogravimetric analysis

Thermogravimetric analysis of the mixture of PS and oxygen carrier was performed under atmospheric pressure by using a TGA/DTA analyzer (SDT Q600, TA instruments). The PS and metal ferrite were homogenized via mortar and pestle with a mass ratio of 1:15 biomass to oxygen carrier. Then, approximately 15 mg of mixture was loaded in TGA and heated to 900 °C at 30 °C/min in nitrogen atmosphere with a flow rate of 100 ml/min. Once the temperature reached 900 °C, the samples were held this temperature for 15 min. Finally, the nitrogen flow was switched to air flow at 100 ml/min for 15 min in order to oxidize the reduced oxygen carrier.

### 2.4. Fluidized bed tests

CLC experiments with PS were conducted in a fluidized bed reaction system, as shown in Fig. 1. The reaction system consisted of a biomass feeder, carrier gas unit, fluidized bed reactor, cyclone separator, condenser, gas flow meter and gas analyzer. A stainless steel tube (i.d. = 26 mm, length = 1000 mm) was used as the fluidized bed reactor. A porous distributor plate was placed in the reactor 600 mm from the top. A K-type thermocouple was used to measure the temperature of the reactor.

At the start of each run, 2.0 g of PS feedstock was load in the biomass feeder (PEF-90AL, Sanki Co. LTD, Japan). The feeding rate was set to 0.20 g/min by a digital controller. A sample of 30.0 g of oxygen carrier particles was loaded on the porous distributor plate in the reactor. Then, the fluidized bed reactor was heated from room temperature to the desired temperature by an electrical furnace with a ramp rate of 10 °C/min in air (600 ml/min). After achieving the desired temperature, the fluidized bed reactor was flushed using nitrogen (99.99%, 600 ml/min) for 5 min to ensure an inert atmosphere. Subsequently, the biomass feeder was turned on, and the PS (2.0 g) was continuously fed into the fluidized bed reactor at a rate of 0.20 g/min. During the feeding period, a nitrogen flow (about 80 ml/min) was used as balance which was intro-

**Table 1**  
Properties of pine sawdust (wt%, air-dried basis).

Ultimate analysis <sup>b</sup>					Proximate analysis <sup>c</sup>			
C	H	N	O <sup>a</sup>	S	Moisture	Volatile	Ash	Fixed carbon
47.16	6.21	0.17	45.22	0.15	6.90	77.96	1.09	14.05

<sup>a</sup> By difference.

<sup>b</sup> Measured by elemental analyzer (Vario Micro cube, Elementar).

<sup>c</sup> Measured by thermogravimetric analyzer (TGA 2000, Las Navas).

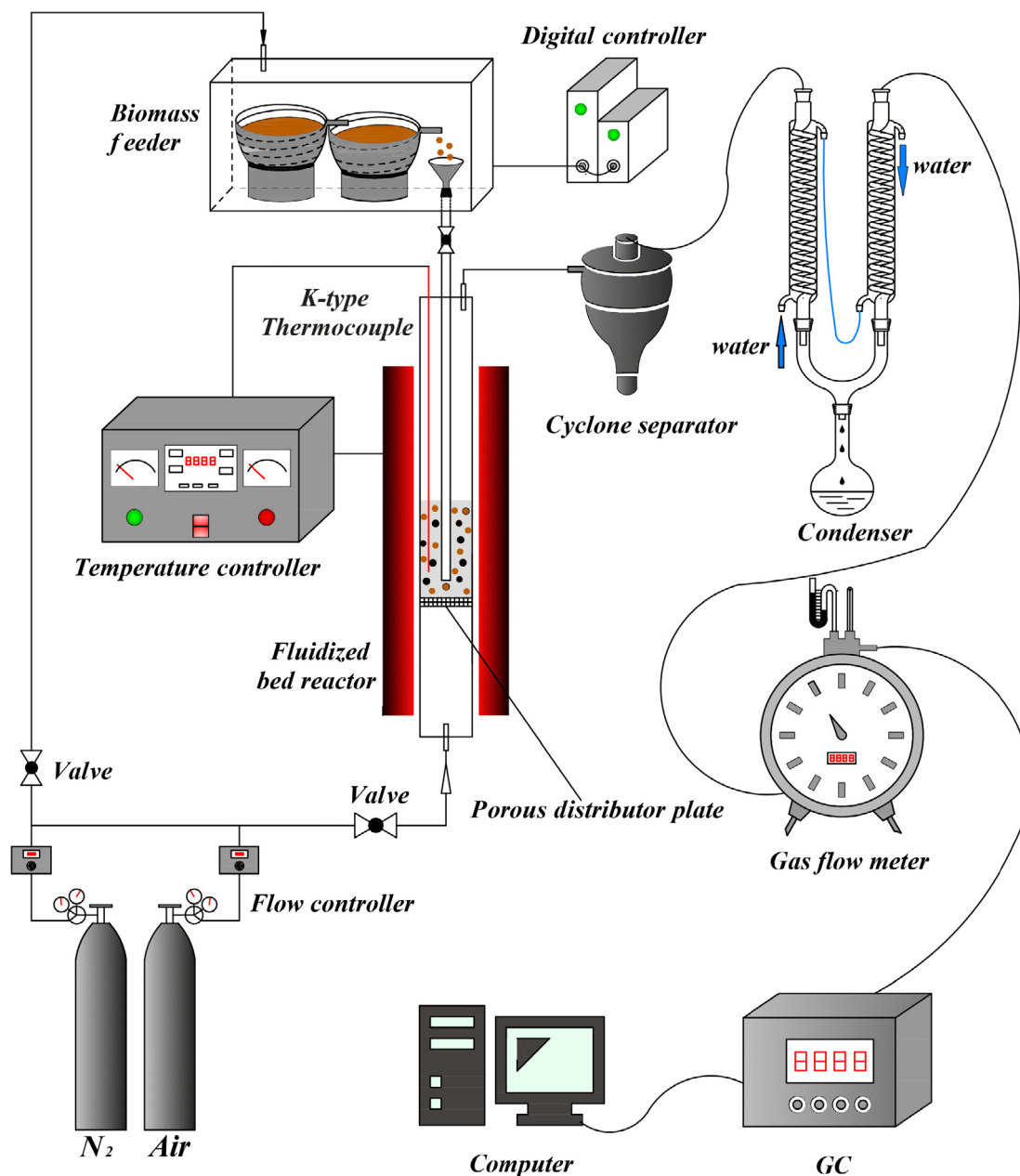


**Fig. 1.** Schematic layout of the laboratory fluidized bed.

duced into the biomass feeder by valve adjustment. Thus, the PS was pushed by nitrogen flow into the fluidized bed reactor through a drop tube. The reaction of PS with oxygen carrier was deemed complete after 30 min. Then, the nitrogen was switched to air (600 ml/min) for 15 min to oxidize the reduced oxygen carrier. Each experiment was repeated three times to ensure the repeatability of the process, and average values were obtained.

The flue gases passed through a cyclone separator to remove fine particles, which was heat-insulated to avoid the condensation of tar. Subsequently, the flue gases flowed into a condenser, and a mixture liquid (including water and tar) was obtained. The total volume of flue gases was determined by a gas flow meter. Then, the gases were introduced into a sample bag. A gas chromatograph (SP-2100A, Beijing Beifen-Ruili analytical instrument Co. Ltd,

**Table 2**  
Species considered in the HSC calculations for  $MFe_2O_4$  (M = Cu, Ni and Co).

Species
C(s), C(g), C <sub>2</sub> (g), C <sub>3</sub> (g), C <sub>4</sub> (g), C <sub>5</sub> (g), CO(g), CO <sub>2</sub> (g), CH <sub>4</sub> (g), C <sub>2</sub> H <sub>2</sub> (g), C <sub>2</sub> H <sub>4</sub> (g), C <sub>2</sub> H <sub>6</sub> (g);
H(g), H <sub>2</sub> (g), H <sub>2</sub> O(g), H <sub>2</sub> O(l), H <sub>2</sub> S(g); O(g), O <sub>2</sub> (g),
S(s), S(g), S <sub>2</sub> (g), S <sub>3</sub> (g), S <sub>4</sub> (g), S <sub>5</sub> (g), S <sub>6</sub> (g), S <sub>7</sub> (g), S <sub>8</sub> (g), SO <sub>2</sub> (g), SO <sub>3</sub> (g), COS(g), CS <sub>2</sub> (g);
N(g), N <sub>2</sub> (g), NH <sub>3</sub> (g), NO(g), NO <sub>2</sub> (g), N <sub>2</sub> O(g), N <sub>2</sub> O <sub>5</sub> (g);
Fe, FeO, Fe <sub>2</sub> O <sub>3</sub> , Fe <sub>3</sub> O <sub>4</sub> , FeCO <sub>3</sub> , FeSO <sub>4</sub> , FeS, FeS <sub>2</sub> , Fe <sub>2</sub> S, Fe <sub>3</sub> C
<i>Ni-containing species</i>
Ni, NiCO <sub>3</sub> , Ni(NO <sub>3</sub> ) <sub>2</sub> , NiFe <sub>2</sub> O <sub>4</sub> , NiO, NiSO <sub>4</sub> , NiS, NiS <sub>2</sub> , Ni <sub>3</sub> S <sub>2</sub> , Ni <sub>3</sub> C, Ni <sub>3</sub> S, Ni <sub>3</sub> S <sub>2</sub> , Ni <sub>3</sub> S <sub>2</sub>
<i>Co-containing species</i>
CoCO <sub>3</sub> , CoFe <sub>2</sub> O <sub>4</sub> , CoO, Co <sub>3</sub> O <sub>4</sub> , CoCO <sub>3</sub> , Co(NO <sub>3</sub> ) <sub>2</sub> , CoO, Co <sub>3</sub> O <sub>4</sub> , CoSO <sub>4</sub> , CoS, CoS <sub>2</sub> , Co <sub>3</sub> S <sub>4</sub> , Co <sub>3</sub> N, Co <sub>2</sub> C, Co
<i>Cu-containing species</i>
Cu, CuO, Cu <sub>2</sub> O, CuFe <sub>2</sub> O <sub>4</sub> , CuFe <sub>2</sub> O <sub>4</sub> , CuCO <sub>3</sub> , Cu(NO <sub>3</sub> ) <sub>2</sub> , CuSO <sub>4</sub> , Cu <sub>2</sub> SO <sub>4</sub> , CuFeS <sub>2</sub> , Cu <sub>5</sub> FeS <sub>4</sub> , CuS, Cu <sub>2</sub> S

China) was used to analyze the gas component. In this study, both the SO<sub>x</sub> and NO<sub>x</sub> were not taken into account due to their low abundance in PS (Table 1).

After every experiment, the mixture liquid in the condenser was collected and sealed storage in a reagent bottle. As the tar yield is relative low in a single test at high temperature, three bottles liquid obtained from three repeated experiments were mixed and further separated into water and tar using the standard ASTM D244 and IP 291.1 methods [31]. The total mass of tar was accurately weighted, and the tar yield in each test was calculated.

### 2.5. Thermodynamic simulation

Based on minimization of Gibbs free energy, thermodynamic simulation of the reaction of  $MFe_2O_4$  (M = Cu, Ni and Co) with PS was performed using equilibrium software HSC-Chemistry 6.0. Thermodynamic equilibrium calculation was beneficial to investigate the species evolution of metal ferrites after the reduction reaction. In the process of thermodynamic simulation, PS was deemed to consist of five basic elements: hydrogen, carbon, oxygen, sulfur,

and nitrogen. The effect of ash on the reaction was not considered due to the low ash content of the PS. All species are shown in Table 2.

### 2.6. Data analysis

The N<sub>2</sub> was used as fluidized gas and its flow was a constant, thus the volume of N<sub>2</sub>,  $v_{N_2}$  (Nm<sup>3</sup>), was calculated in the flue gas. The total volume of flue gas,  $v_{out}$  (Nm<sup>3</sup>), was measured by the gas flow meter, or was calculated as the balance of N<sub>2</sub> flow:

$$v_{out} = \frac{v_{N_2}}{1 - \sum_i x_i} \quad (1)$$

where  $x_i$  represents the molar percentages of the gas component ( $i = CO_2, CO, CH_4, H_2, C_2H_4$  and  $C_2H_6$ ) in the flue gas. The  $v_{out}$  and  $v_{N_2}$  are the volumes of flue gas and N<sub>2</sub>, respectively.

The volume of gas products ( $v_g$ , Nm<sup>3</sup>) was calculated by

$$v_g = v_{out} \sum_i x_i \quad (2)$$

The carbon conversion ( $x_c$ , %) was introduced to illustrate the conversion degree of carbon in PS into carbonaceous gases in fuel reactor, and it was calculated as

$$x_c = \frac{12 v_{out} (x_{CO} + x_{CO_2} + x_{CH_4} + 2(x_{C_2H_4} + x_{C_2H_6}))}{22.4 \times C\% \times m_b} \times 100\% \quad (3)$$

where  $m_b$  (kg) denotes the mass of PS in each test, and C% is the mass percentage of carbon in PS.

The CO<sub>2</sub> capture efficiency ( $\eta_{CO_2}$ , %) was defined as the conversion degree of carbonaceous gases into CO<sub>2</sub> in the fuel reactor, and it was calculated as

$$\eta_{CO_2} = \frac{x_{CO_2}}{x_{CO} + x_{CH_4} + x_{CO_2} + 2(x_{C_2H_4} + x_{C_2H_6})} \times 100\% \quad (4)$$

The tar yield (g/Nm<sup>3</sup>) is defined as the ratio of the mass of tar to the volume of gas products in each run. It was calculated as

$$Tar\ yield = \frac{M_{tar}}{3 v_g} \quad (5)$$

where  $M_{tar}$  is the total mass of tar obtained from three repeated experiments.

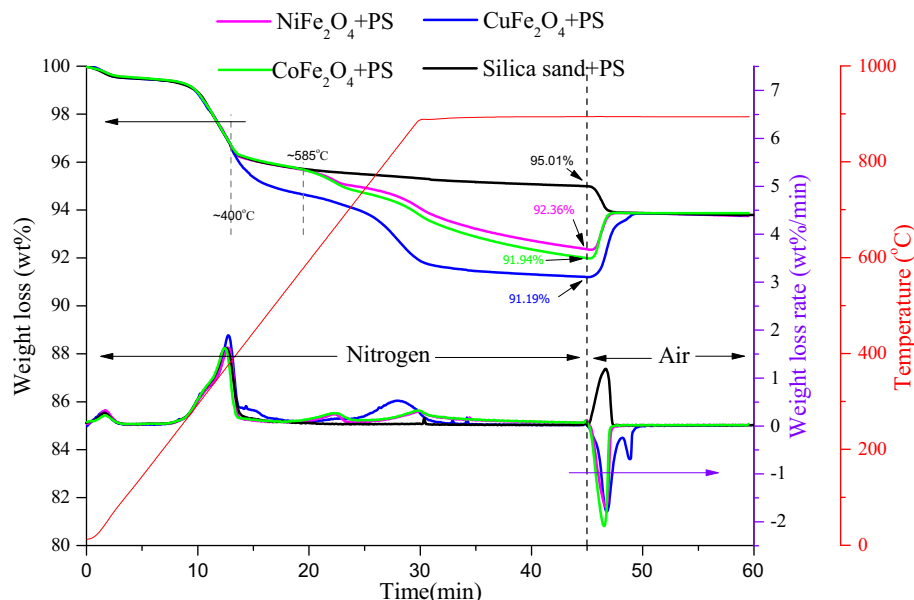


**Fig. 2.** TG/DTG curves for mixture of PS and  $MFe_2O_4$  (M = Cu, Ni and Co).

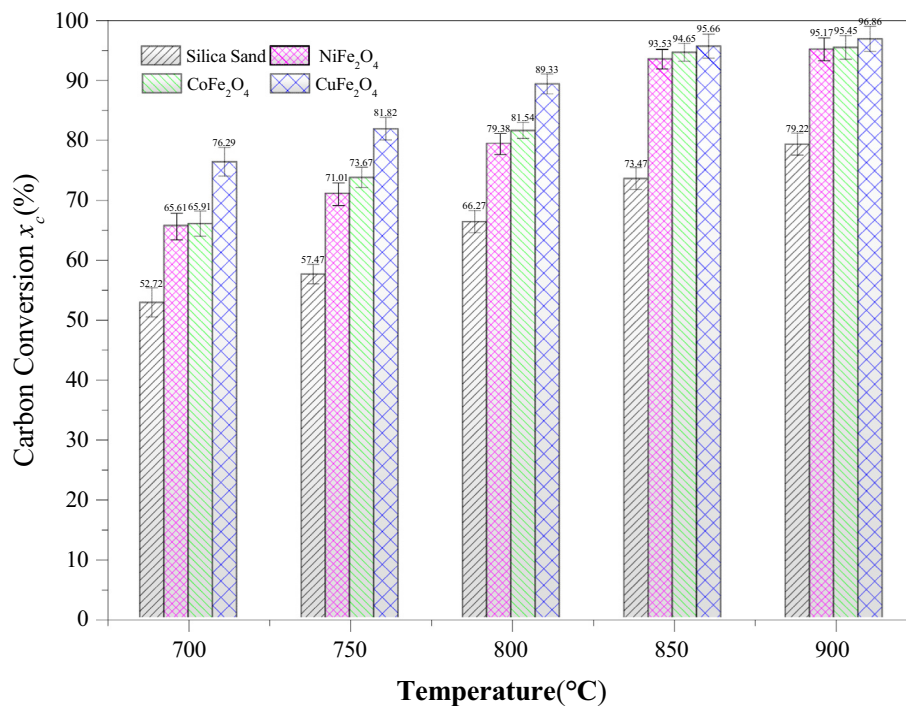


Fig. 3. Effects of the temperature on the carbon conversion for different metal ferrites.

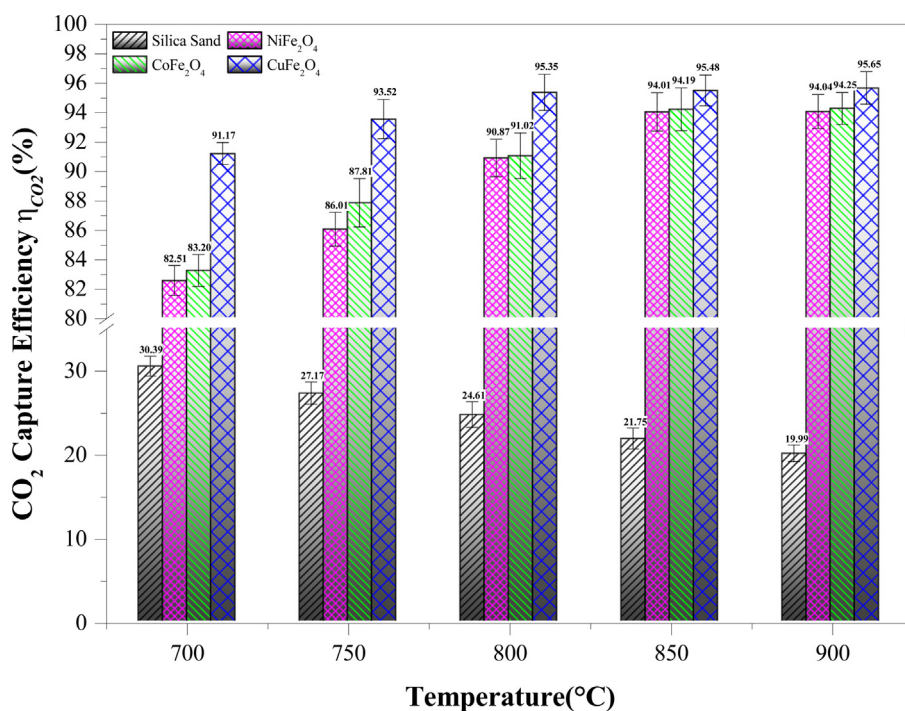


Fig. 4. Effects of the temperature on CO<sub>2</sub> capture efficiency for different metal ferrites.

### 2.7. Characterization of properties

X-ray powder diffraction (XRD) patterns of three metal ferrites were obtained by using an X'Pert PRO, (PAN alytical B.V.) with Cu  $K\alpha$  radiation and indexed in comparison to the JCPDS files. The samples were scanned from  $2\theta = 10^\circ$  to  $80^\circ$  at  $0.0167^\circ$  steps, and the Scherrer's Formulae [32] was used to calculated the

crystallite size of metal ferrites. The specific area, total pore volume and average pore diameter of the metal ferrites were determined by N<sub>2</sub> adsorption-desorption at  $-196^\circ\text{C}$  using accelerated surface area porosimetry (ASAP 2010, Micrometrics) instruments. Scanning electron microscopy (SEM) (FEI-Quanta 200) was utilized to characterize the surface morphology of the metal ferrites.

### 3. Results and discussion

#### 3.1. Thermogravimetric analysis

The weight loss of the mixture of PS and oxygen carrier during reduction and oxidation processes is shown in Fig. 2. In the reduction process, compared with the PS pyrolysis (i.e., using silica sand as bed material), a significant change in weight loss was observed at approximately 400 °C when using  $\text{CuFe}_2\text{O}_4$  as an oxygen carrier. This result indicated that the initial reaction temperature of  $\text{CuFe}_2\text{O}_4$  was round 400 °C. It can be concluded that no reactions between PS with  $\text{CuFe}_2\text{O}_4$  occur when the temperature is below 400 °C, and the weight loss of the mixture is mainly attributed to moisture drying and devolatilization of PS. At temperatures greater than 400 °C, the  $\text{CuFe}_2\text{O}_4$  reacted with the volatiles and residual char. For  $\text{NiFe}_2\text{O}_4$  and  $\text{CoFe}_2\text{O}_4$ , the TGA curves were similar, and the initial reaction temperatures were approximately 585 °C, higher than that of  $\text{CuFe}_2\text{O}_4$ .

From the DTG curves, two characteristic temperatures  $T_m$  (namely the temperature corresponding the peak value of DTG) were approximately 450 °C and 835.5 °C for  $\text{CuFe}_2\text{O}_4$ , 662.1 °C and 889.5 °C for  $\text{CoFe}_2\text{O}_4$ , 663.6 °C and 890.5 °C for  $\text{NiFe}_2\text{O}_4$ . This further confirmed that the  $\text{CuFe}_2\text{O}_4$  exhibited a lower reduction temperature compared to that of  $\text{NiFe}_2\text{O}_4$  and  $\text{CoFe}_2\text{O}_4$ . The final weight loss of the mixture of PS with  $\text{CuFe}_2\text{O}_4$ , PS with  $\text{CoFe}_2\text{O}_4$ , and PS with  $\text{NiFe}_2\text{O}_4$  was 8.81 wt%, 8.06 wt% and 7.44 wt%, respectively. Meanwhile, the maximum weight loss rates were 0.529 wt%/min for  $\text{CuFe}_2\text{O}_4$ , 0.314 wt%/min for  $\text{CoFe}_2\text{O}_4$  and 0.307 wt%/min for  $\text{NiFe}_2\text{O}_4$ . These results indicated that the reactivity of the  $\text{MFe}_2\text{O}_4$  ( $M = \text{Cu}, \text{Ni}$  and  $\text{Co}$ ) decreased in the following order:  $\text{CuFe}_2\text{O}_4 > \text{CoFe}_2\text{O}_4 > \text{NiFe}_2\text{O}_4$ . Banerjee et al. [26] and Kang et al. [33] reported that the higher reactivity of  $\text{CuFe}_2\text{O}_4$  may be attributed to the high reducible  $\text{Cu}^{2+}$  in the spinel structure, improving reduction kinetics and enhancing the reducibility of  $\text{Fe}^{3+}$ . Shin et al. [34] also reported that  $\text{CuFe}_2\text{O}_4$  was more readily reduced than  $\text{NiFe}_2\text{O}_4$ .

In the oxidation process, the weight of silica sand and PS mixture decreased due to the combustion of residual char. Alternatively, the weight of metal ferrites and PS mixture decreased slightly at first due to residual char combustion and then increased remarkably as the reduced metal ferrites were oxidized by air. Additionally, it is clear that the reduced  $\text{CoFe}_2\text{O}_4$  was first oxidized to the stable state, followed by  $\text{NiFe}_2\text{O}_4$  and  $\text{CuFe}_2\text{O}_4$ . The minimum value of the weight loss rate was  $-2.097$  wt%/min,  $-1.798$  wt%/min and  $-1.703$  wt%/min for  $\text{CoFe}_2\text{O}_4$ ,  $\text{CuFe}_2\text{O}_4$  and  $\text{NiFe}_2\text{O}_4$ , respectively. This result implied that the oxidation uptake rate of  $\text{CoFe}_2\text{O}_4$  was higher than that of  $\text{NiFe}_2\text{O}_4$  and  $\text{CuFe}_2\text{O}_4$ , and a similar result was reported by Fan et al. [35]. The DTG curve of  $\text{CuFe}_2\text{O}_4$  showed two peaks in the oxidation process that may be due to the oxidation of the reduced products, including  $\text{Cu}$ ,  $\text{Fe}_3\text{O}_4$  and  $\text{CuFeO}_2$  (Fig. 6(a)), at different oxygen partial pressures [36].

#### 3.2. Fluidized bed results

##### 3.2.1. Effects of temperature on carbon conversion ( $x_c$ )

In the biomass CLC process, temperature not only affects the reactivity of oxygen carriers but also influences the pyrolysis/gasification process of biomass. As shown in Fig. 3,  $x_c$  increased from 52.72% to 79.72%, 65.61% to 95.17%, 65.91% to 95.45%, and 76.29% to 96.86% for silica sand,  $\text{NiFe}_2\text{O}_4$ ,  $\text{CoFe}_2\text{O}_4$  and  $\text{CuFe}_2\text{O}_4$ , respectively, as the reaction temperature increased from 750 °C to 900 °C in 50 °C increments. Compared with the process of PS pyrolysis, the presence of metal ferrites significantly improved the  $x_c$ . The reaction reactivity of PS and metal ferrites were enhanced at higher temperatures, which resulted in increasing  $x_c$  with increasing temperature. When  $\text{CoFe}_2\text{O}_4$  was used as an oxygen carrier, the  $x_c$  of PS was slightly higher than that of PS when  $\text{NiFe}_2\text{O}_4$  was used at the whole temperature range. At a temperature range from 700 °C to 800 °C, the  $x_c$  of PS was significantly higher when using  $\text{CuFe}_2\text{O}_4$  as oxygen carrier than when  $\text{NiFe}_2\text{O}_4$  and  $\text{CoFe}_2\text{O}_4$  were used. Alternatively, there were no significant differences in  $x_c$  when different oxygen carriers were used at the

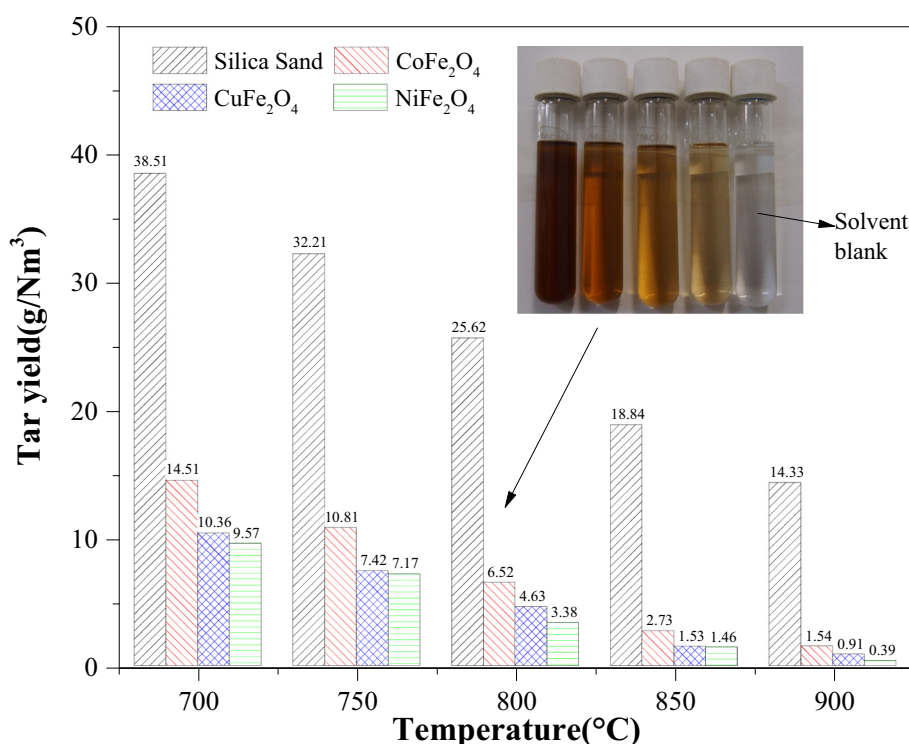


Fig. 5. Effects of temperature on tar yield for different metal ferrites.

temperature range from 850 °C to 900 °C. This was mainly attributed to the higher reactivity of  $\text{CuFe}_2\text{O}_4$  at relatively lower temperatures, which was confirmed by TGA results. The reactivity of metal ferrites significantly increased with temperature, while no effect of temperature on  $x_c$  was observed. At the same temperatures, the values of  $x_c$  of PS for three metal ferrites increased in the following order:  $\text{NiFe}_2\text{O}_4 < \text{CoFe}_2\text{O}_4 < \text{CuFe}_2\text{O}_4$ , which is in agreement with TGA results.

### 3.2.2. Effects of the temperature on carbon capture efficiency ( $\eta_{\text{CO}_2}$ )

As illustrated in Fig. 4, the  $\eta_{\text{CO}_2}$  decreased with increasing temperature in the PS pyrolysis process. This result was mainly due to the favorable high temperature of the Boudouard reaction [37], which resulted in a portion of  $\text{CO}_2$  consumed as a gasification medium. For three oxygen carriers, the  $\eta_{\text{CO}_2}$  increased at first and then plateaued as temperature increased. The increasing trend can be explained by the reactivity of metal ferrites increased with the increasing temperature, which resulted in high concentration of  $\text{CO}_2$  was achieved. However, an increasing amount of pyrolysis products were generated with increasing temperature, which resulted in an insufficient oxygen level at high temperatures. Additionally, volatiles were released quickly at higher reaction temperatures; thus, a percentage of volatiles escaped from the reactor before reacting with metal ferrites. Therefore, the  $\eta_{\text{CO}_2}$  was relatively stable at high temperatures without great fluctuations.

When using  $\text{CoFe}_2\text{O}_4$  as an oxygen carrier, the  $\eta_{\text{CO}_2}$  was slightly higher compared with the  $\text{NiFe}_2\text{O}_4$ . It was noted that the  $\eta_{\text{CO}_2}$  of  $\text{CuFe}_2\text{O}_4$  was far higher than that of  $\text{CoFe}_2\text{O}_4$  and  $\text{NiFe}_2\text{O}_4$  at a lower temperature, while the differences of  $\eta_{\text{CO}_2}$  between  $\text{CuFe}_2\text{O}_4$  and two other metal ferrites were decreased gradually with the increasing temperature. For example, the  $\eta_{\text{CO}_2}$  at 700 °C of  $\text{CuFe}_2\text{O}_4$ ,  $\text{CoFe}_2\text{O}_4$  and  $\text{NiFe}_2\text{O}_4$  was 91.17%, 83.20% and 82.51%, respectively, while the  $\eta_{\text{CO}_2}$  at 850 °C for  $\text{CuFe}_2\text{O}_4$ ,  $\text{CoFe}_2\text{O}_4$  and  $\text{NiFe}_2\text{O}_4$  was 95.48%, 94.19% and 94.01%, respectively. Furthermore, the maximum values of  $\eta_{\text{CO}_2}$  at 900 °C were 95.65%, 94.25%, and 94.04% for  $\text{CuFe}_2\text{O}_4$ ,  $\text{CoFe}_2\text{O}_4$  and  $\text{NiFe}_2\text{O}_4$ , respectively. No significant change of  $\eta_{\text{CO}_2}$  was observed with a temperature increase from 850 °C to 900 °C. When  $\text{CuFe}_2\text{O}_4$  was used, the  $\eta_{\text{CO}_2}$  maintained a comparatively high percentage across the temperature range, which increased slightly from 91.17% at 700 °C to 95.65% at 900 °C. Thus, the effect of temperature on the  $\eta_{\text{CO}_2}$  for  $\text{CuFe}_2\text{O}_4$  was not obvious compared to  $\text{CoFe}_2\text{O}_4$  and  $\text{NiFe}_2\text{O}_4$ . These results indicated that the  $\text{CuFe}_2\text{O}_4$  has a higher reactivity, and it can be used in biomass CLC for  $\text{CO}_2$  capture at a relative lower temperature compared with  $\text{CoFe}_2\text{O}_4$  and  $\text{NiFe}_2\text{O}_4$ .

### 3.2.3. Effects of the temperature on tar yield

In general, the catalytic activity of the metal ferrites depends mainly on the distribution of the cations in the spinel structure [38]. The cations located at octahedral sites are almost exclusively exposed on the surface of the spinel crystallites, and thus, exhibit catalytic activity [39]; while the cations located at tetrahedral positions have no catalytic activity.

As the reactor temperature elevated from 700 °C to 900 °C, the tar yield decreased from 38.51 g/Nm<sup>3</sup> to 14.33 g/Nm<sup>3</sup>, 14.51 g/Nm<sup>3</sup> to 1.54 g/Nm<sup>3</sup>, 10.36 g/Nm<sup>3</sup> to 0.91 g/Nm<sup>3</sup>, and 9.57 g/Nm<sup>3</sup> to 0.39 g/Nm<sup>3</sup> for silica sand,  $\text{CuFe}_2\text{O}_4$ ,  $\text{CoFe}_2\text{O}_4$  and  $\text{NiFe}_2\text{O}_4$ , respectively (Fig. 5). At the same temperatures, the tar yield decreased in the following order:  $\text{CuFe}_2\text{O}_4 > \text{CoFe}_2\text{O}_4 > \text{NiFe}_2\text{O}_4$ . These results indicated that the presence of metal ferrites significantly enhanced the decomposition of tar. This effect was mainly attributed to the ability of metal ferrites to act as oxygen carriers and provide oxygen for tar combustion. Simultaneously, they can act as catalysts for the decomposition of tar. The decomposition of tar was accelerated by increasing temperature, primarily due to reforming and

cracking of tar as well as enhanced reactivity of oxygen carriers at high temperatures.

It was noted that the reactivity of  $\text{NiFe}_2\text{O}_4$  was lower than that of  $\text{CuFe}_2\text{O}_4$  and  $\text{CoFe}_2\text{O}_4$ . However, when using  $\text{NiFe}_2\text{O}_4$  as an oxygen carrier, the tar yield was lowest under identical conditions. Therefore, we inferred that  $\text{NiFe}_2\text{O}_4$  has a higher catalytic reactivity for tar cracking and reforming compared with  $\text{CoFe}_2\text{O}_4$  and  $\text{CuFe}_2\text{O}_4$ , which may be due to the formation of Ni metal in the reduction

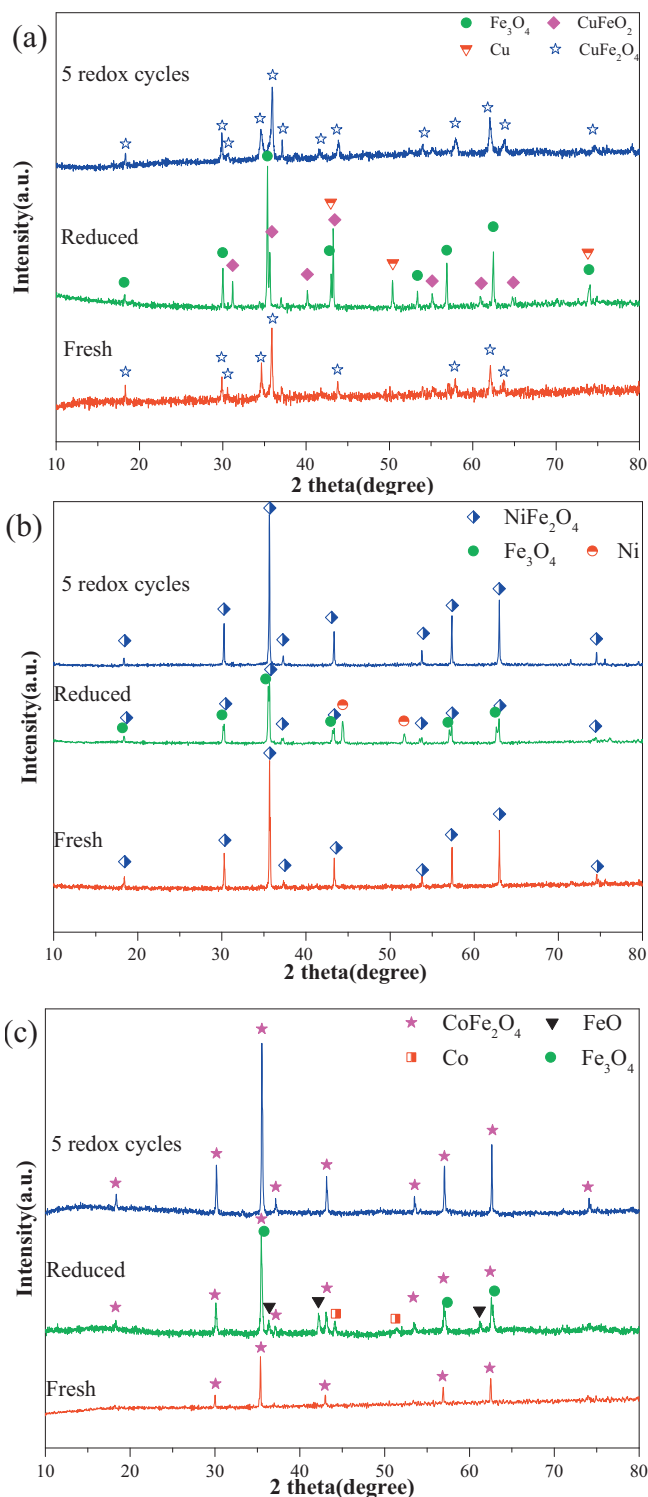


Fig. 6. XRD patterns of fresh, reduced, and after five cycles metal ferrites:  $\text{CuFe}_2\text{O}_4$  (a),  $\text{NiFe}_2\text{O}_4$  (b), and  $\text{CoFe}_2\text{O}_4$  (c).

**Table 3**  
Experimental results of multiple redox cycles at 850 °C.

Cycle	Carbon conversion $x_c$ (%)			Carbon capture efficiency $\eta_{CO_2}$ (%)		
	CuFe <sub>2</sub> O <sub>4</sub>	NiFe <sub>2</sub> O <sub>4</sub>	CoFe <sub>2</sub> O <sub>4</sub>	CuFe <sub>2</sub> O <sub>4</sub>	NiFe <sub>2</sub> O <sub>4</sub>	CoFe <sub>2</sub> O <sub>4</sub>
1st	95.66	93.53	94.65	95.48	94.04	94.19
2nd	95.51	91.84	93.78	94.98	92.59	94.07
3rd	95.46	88.53	93.89	93.65	89.98	93.48
4th	94.88	86.38	93.21	93.76	87.15	93.40
5th	94.90	83.85	93.47	93.81	86.30	93.51

**Table 4**  
Characteristics of fresh and used oxygen carrier particles after five cycles.

	Specific area (m <sup>2</sup> /g)		Total pore volume (cm <sup>3</sup> /g)		Average pore diameter (nm)		Crystallite size <sup>d</sup> (nm)	
	Fresh	Used	Fresh	Used	Fresh	Used	Fresh	Used
CuFe <sub>2</sub> O <sub>4</sub>	1.418	1.832	0.0062	0.0098	17.355	14.756	58.47	66.93
NiFe <sub>2</sub> O <sub>4</sub>	10.219	1.668	0.0086	0.0045	3.185	18.509	102.27	106.99
CoFe <sub>2</sub> O <sub>4</sub>	6.447	5.817	0.0147	0.0110	6.202	9.958	102.17	106.95

<sup>d</sup> Calculated from (211) peak of CuFe<sub>2</sub>O<sub>4</sub>, (311) peak of CoFe<sub>2</sub>O<sub>4</sub> and NiFe<sub>2</sub>O<sub>4</sub> using the Scherrer equation.

process (Fig. 6(b)). In addition, a portion of NiFe<sub>2</sub>O<sub>4</sub> remained after reduction; in other words, the residual NiFe<sub>2</sub>O<sub>4</sub> also maintained catalytic activity to some extent. Similar to NiFe<sub>2</sub>O<sub>4</sub>, a portion of CoFe<sub>2</sub>O<sub>4</sub> remained in the reduced samples when CoFe<sub>2</sub>O<sub>4</sub> was used (Fig. 6(c)); while the spinel structure of CuFe<sub>2</sub>O<sub>4</sub> disappeared after reduction (Fig. 6(a)), which may have resulted in a decrease of catalytic activity. Therefore, although the CoFe<sub>2</sub>O<sub>4</sub> showed higher tar yield than CuFe<sub>2</sub>O<sub>4</sub> at the same temperature, we still cannot conclude that the catalytic performance of CoFe<sub>2</sub>O<sub>4</sub> is lower than that of CuFe<sub>2</sub>O<sub>4</sub> because the lower tar yield may be due to combustion instead of catalysis. In the future, we aim to evaluate the catalytic activity of three metal ferrites for the decomposition of tar.

### 3.2.4. Experiments with multiple redox cycles

Reactivity and stability are very important properties of oxygen carriers. In order to study the reusability of the three oxygen carriers, five redox cycled experiments were conducted in a fluidized bed at 850 °C. A sample of metal ferrites (30.0 g) was used. In the start of each run, PS (2.0 g) was fed into the reactor with a feeding rate 0.20 g/min. Once each run finished, the regenerated oxygen carrier was recycled for the next experiment, and the ash was not separated from the reactor. The resulting  $x_c$  and  $\eta_{CO_2}$  values are listed in Table 3.

After five redox cycles, the  $x_c$  and  $\eta_{CO_2}$  decreased from 96.66% to 94.90% and 95.88% to 93.81% for CuFe<sub>2</sub>O<sub>4</sub>, 93.53% to 83.85% and 94.04% to 86.30% for NiFe<sub>2</sub>O<sub>4</sub>, and 94.65% to 93.47% and 94.19% to 93.51% for CoFe<sub>2</sub>O<sub>4</sub>, respectively. For the CuFe<sub>2</sub>O<sub>4</sub> and CoFe<sub>2</sub>O<sub>4</sub>, both  $x_c$  and  $\eta_{CO_2}$  remained steady and were maintained at a higher percentage after five cycles; while the  $x_c$  and  $\eta_{CO_2}$  decreased sharply when the NiFe<sub>2</sub>O<sub>4</sub> was used. These results suggest that the reactivity of NiFe<sub>2</sub>O<sub>4</sub> decreased after five cycles; while CuFe<sub>2</sub>O<sub>4</sub> and CoFe<sub>2</sub>O<sub>4</sub> have excellent cycling performance.

Although five consecutive cycles are not enough to deliver the stability of the oxygen carriers, a couple of cycles in the beginning will strongly effect on the structure of the oxygen carriers. By observing the data in Table 3, we inferred that CuFe<sub>2</sub>O<sub>4</sub> and CoFe<sub>2</sub>O<sub>4</sub> were more stable and better suited for biomass CLC for CO<sub>2</sub> capture compared with NiFe<sub>2</sub>O<sub>4</sub>.

## 3.3. The results of characterization of oxygen carriers

### 3.3.1. XRD

The fresh, reduced, and five redox-cycled oxygen carriers at 850 °C were examined by XRD. As shown in Fig. 6, XRD patterns revealed that all diffraction peaks of metal ferrites were indexed

in comparison to JCPDS files (JCPDS card No. 34-0425 for CuFe<sub>2</sub>O<sub>4</sub>, 22-1086 for CoFe<sub>2</sub>O<sub>4</sub>, and 44-1485 for NiFe<sub>2</sub>O<sub>4</sub>, respectively). The CuFe<sub>2</sub>O<sub>4</sub> has a tetragonal distorted inverse spinel structure; while CoFe<sub>2</sub>O<sub>4</sub> and NiFe<sub>2</sub>O<sub>4</sub> have a cubic inverse spinel structure. Therefore, the CuFe<sub>2</sub>O<sub>4</sub> has a lower symmetry than CoFe<sub>2</sub>O<sub>4</sub> and NiFe<sub>2</sub>O<sub>4</sub>, which can enhance the diffusion and reduction rates of metal ions in spinel structure [26]. From the XRD patterns, the sharp diffraction peaks of fresh MFe<sub>2</sub>O<sub>4</sub> (M = Cu, Ni and Co) revealed well-crystallized structures and demonstrated the sol-gel method is feasible for the preparation of metal ferrites.

From the XRD pattern of the reduced sample of CuFe<sub>2</sub>O<sub>4</sub> (Fig. 6(a)), Cu, Fe<sub>3</sub>O<sub>4</sub> and CuFeO<sub>2</sub> were observed as reduced counterparts. The CuFeO<sub>2</sub> was primarily due to the decomposition of CuFe<sub>2</sub>O<sub>4</sub>. For the NiFe<sub>2</sub>O<sub>4</sub> oxygen carrier (Fig. 6(b)), the reduced products were primarily Ni and Fe<sub>3</sub>O<sub>4</sub>, and similar results have been reported in the literature [33,40]. The XRD patterns in Fig. 6(c) clearly shows that the reduced counterparts were Fe<sub>3</sub>O<sub>4</sub>, FeO and Co when CoFe<sub>2</sub>O<sub>4</sub> was used. The presence of FeO was due to the further reduction of the Fe<sub>3</sub>O<sub>4</sub>. It was noted that the FeO was not observed when the CuFe<sub>2</sub>O<sub>4</sub> and NiFe<sub>2</sub>O<sub>4</sub> were used as oxygen carriers. It was mainly attributed to the ability of Co<sup>2+</sup> in the spinel structure to improve the conversion of Fe<sub>3</sub>O<sub>4</sub> to FeO [26,41]. Furthermore, a percentage of NiFe<sub>2</sub>O<sub>4</sub> and CoFe<sub>2</sub>O<sub>4</sub> remained after the reduction reaction; while the spinel structure of CuFe<sub>2</sub>O<sub>4</sub> disappeared completely. This also confirmed that the CuFe<sub>2</sub>O<sub>4</sub> had higher reactivity. Meanwhile, the disappearance of spinel structure could have resulted in the decrease of catalytic activity.

In comparison with the fresh oxygen carriers, the XRD patterns of three oxygen carriers presented no significant phase change after five redox cycles. This result implied three metal ferrites were regenerated completely. The all crystallite sizes were increased after five redox cycles, as shown in Table 4. Although, there were no indications that metal ferrites had reacted with ash of biomass. This could be attributed to the low abundance of ash was undetectable. On one hand, ash can lead to an agglomeration of the oxygen carrier and defluidization of the fluidized bed [42]; on the other hand, it can also improve the reaction reactivity of the oxygen carrier [43] as well enhance the gasification reaction of biomass as a catalyst to some extent. The role of ash in biomass CLC should be further explored in the future studies.

### 3.3.2. SEM

The SEM images of the fresh oxygen carrier and the used oxygen carrier after five cycles are shown in Fig. 7. The fresh CuFe<sub>2</sub>O<sub>4</sub> oxygen carrier (Fig. 7(a)) was very smooth, exhibiting high uniformity

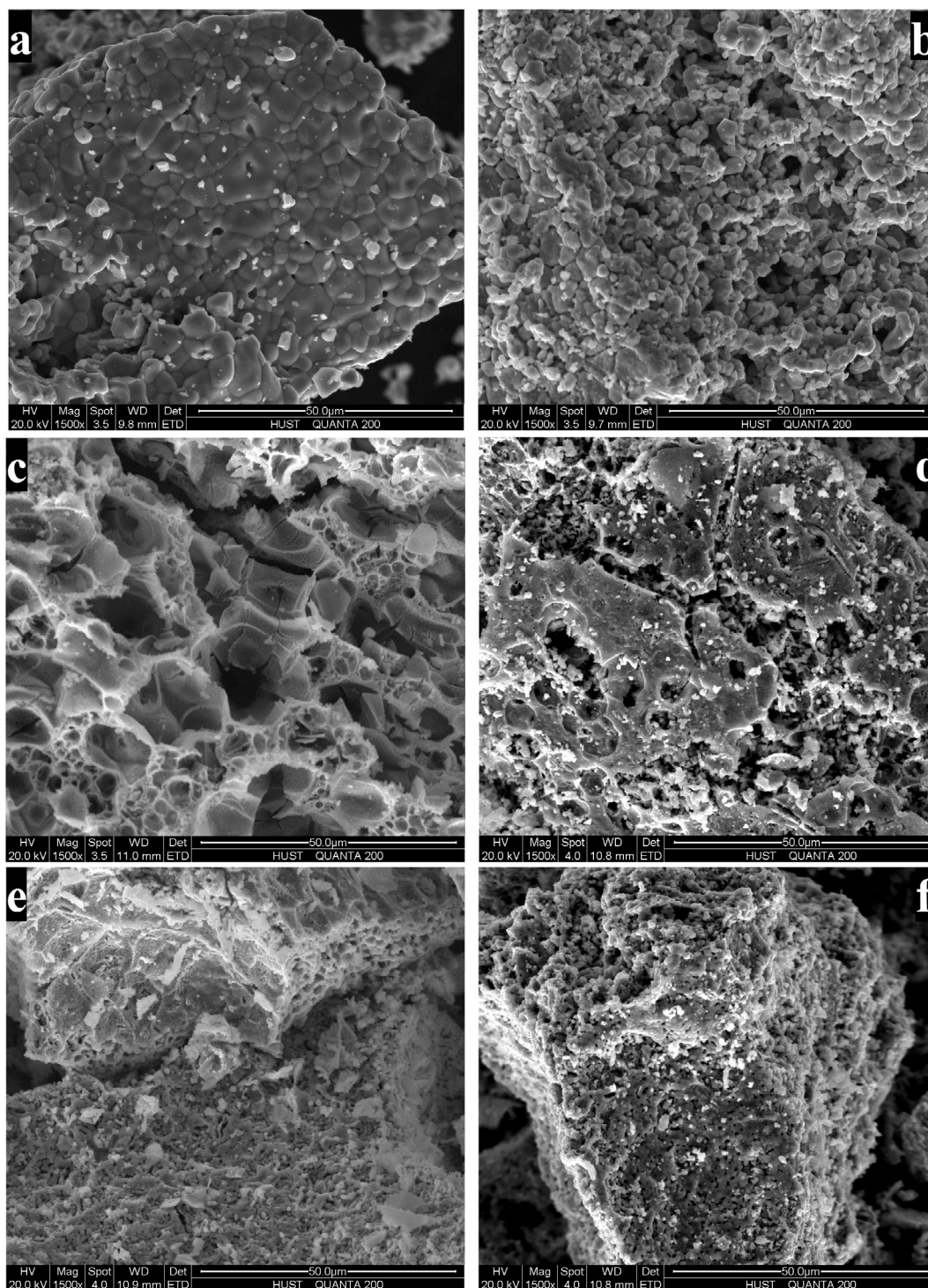


Fig. 7. SEM images of fresh (left) and after five cycles (right) metal ferrites:  $\text{CuFe}_2\text{O}_4$  (a, b),  $\text{NiFe}_2\text{O}_4$  (c, d) and  $\text{CoFe}_2\text{O}_4$  (e, f).

and poor porosity. However, for  $\text{CuFe}_2\text{O}_4$  oxygen carrier after five redox cycles, the surface was uneven and rough (Fig. 7(b)). Meanwhile, a lot of grains were produced, the compact structure was destroyed, and more pores appeared on the surface. This was attributed to a change in the spinel structure from the formation of Cu,  $\text{Fe}_3\text{O}_4$  and  $\text{CuFe}_2\text{O}_4$  in the reduction process. Additionally, lattice oxygen released from  $\text{CuFe}_2\text{O}_4$  could cause the formation of pores. For the fresh  $\text{NiFe}_2\text{O}_4$ , the surface had good porosity with a beehive structure. This is beneficial to the diffusion of pyrolysis gases of PS into the inner of the oxygen carrier. After five redox cycles, the beehive structure was no longer observed, and some

slits formed. It was inferred that the surface sintering of  $\text{NiFe}_2\text{O}_4$  occurred, which resulted in the decrease of  $\text{NiFe}_2\text{O}_4$  reactivity with increasing cycle times, as shown in Table 3. The surface of fresh  $\text{CoFe}_2\text{O}_4$  was coarse and porous. The surface morphology was not significant, meaning no difference between the fresh and used oxygen carriers was observed.

### 3.3.3. BET

Table 4 summarizes the specific areas, total pore volumes, and average pore diameters of the fresh and five redox-cycled oxygen carriers. Specific areas of fresh oxygen carriers were  $1.418 \text{ m}^2/\text{g}$

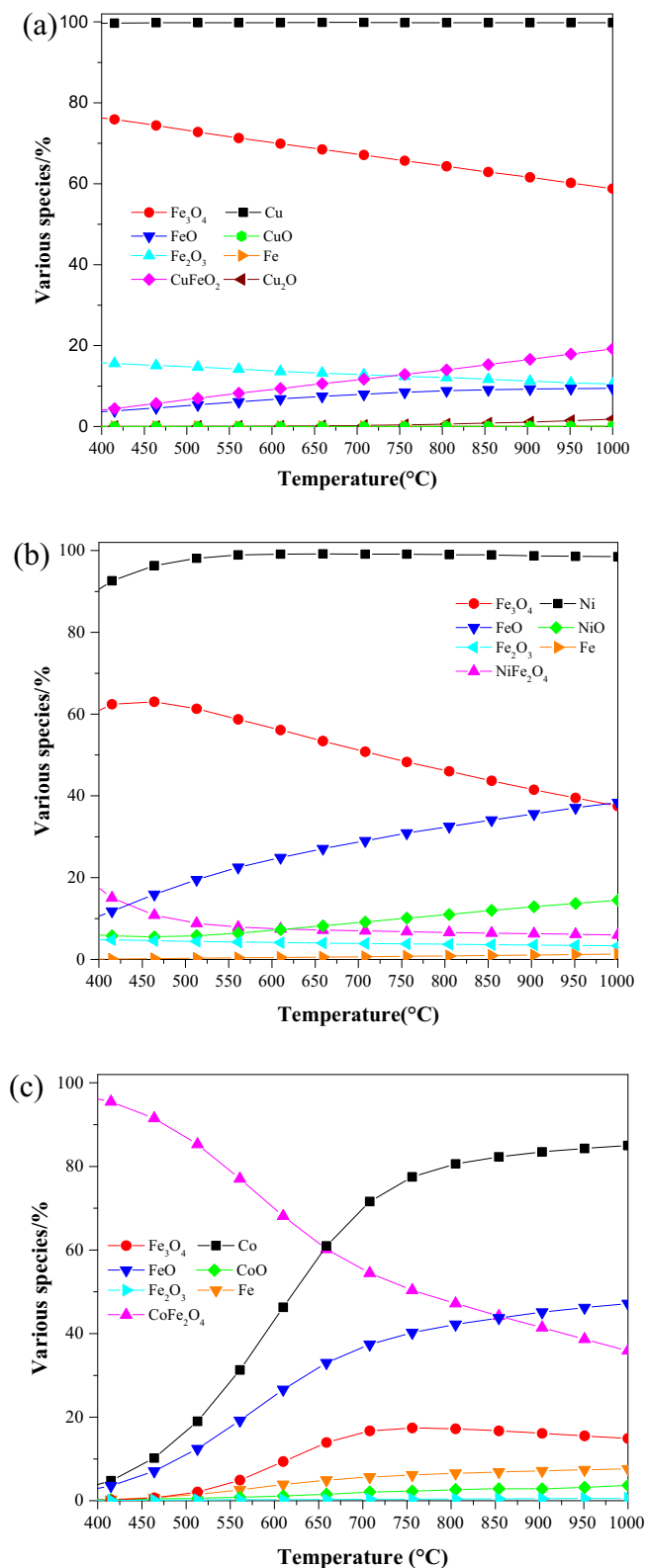


Fig. 8. Equilibrium distribution of various species for the reaction of PS with  $MFe_2O_4$ . (a)  $CuFe_2O_4$ ; (b)  $NiFe_2O_4$ ; (c)  $CoFe_2O_4$ .

for  $CuFe_2O_4$ ,  $6.447 \text{ m}^2/\text{g}$  for  $CoFe_2O_4$  and  $10.219 \text{ m}^2/\text{g}$  for  $NiFe_2O_4$ , respectively. The fresh  $NiFe_2O_4$  had greater specific area than  $CuFe_2O_4$  and  $CoFe_2O_4$ . A greater specific area is beneficial to the reactions of the pyrolysis products with oxygen carriers. After five redox cycles, the specific area of  $CuFe_2O_4$  increased to  $1.832 \text{ m}^2/\text{g}$  due to more pores produced in the reaction process; while the

specific area of  $CoFe_2O_4$  decreased slightly to  $5.817 \text{ m}^2/\text{g}$  may be due to slight sintering. Compared with  $CuFe_2O_4$  and  $CoFe_2O_4$ , the surface area of  $NiFe_2O_4$  decreased significantly from  $10.219 \text{ m}^2/\text{g}$  to  $1.668 \text{ m}^2/\text{g}$  after five cycles. The reduction in pore volume and increase in average pore size further confirmed that significant sintering of  $NiFe_2O_4$  particles occurred after five redox cycles. Combined with the results of cycle tests, we can conclude that both  $CuFe_2O_4$  and  $CoFe_2O_4$  have higher sintering resistance and thermal stability than  $NiFe_2O_4$ .

### 3.4. Thermodynamic simulation

Fig. 8 shows the distribution of equilibrium species after the reaction of PS with  $MFe_2O_4$  ( $M = Cu, Ni \text{ and } Co$ ). According to the results of the thermodynamic simulation,  $CuFe_2O_4$  was not observed in the reduced sample, while  $NiFe_2O_4$  and  $CoFe_2O_4$  were observed across the simulation temperature range, and the percentage of these metal ferrites decreased with increasing temperature. The result indicated that the  $CuFe_2O_4$  more easily reacted with PS in CLC, which agreed well with the results of TGA and fluidized bed tests. High temperature favorably enhanced the reaction reactivity of three metal ferrites. Furthermore, the main reduced counterparts were  $Cu$  and  $CuFeO_2$  for  $CuFe_2O_4$ ,  $Ni$  and  $Fe_3O_4$  for  $NiFe_2O_4$ , and  $Co$ ,  $FeO$  and  $Fe_3O_4$  for  $CoFe_2O_4$ , respectively, which was confirmed by the XRD patterns (Fig. 6).

At the temperature range from  $700 \text{ }^\circ\text{C}$  to  $1000 \text{ }^\circ\text{C}$ , the content of  $FeO$  in the reduced samples increased in the following series:  $CuFe_2O_4 < NiFe_2O_4 < CoFe_2O_4$ , while the opposite was observed for the content of  $Fe_3O_4$  under identical conditions. As temperature increased from  $700 \text{ }^\circ\text{C}$  to  $1000 \text{ }^\circ\text{C}$ , the content of  $FeO$  increased from  $7.89\%$  to  $9.43\%$  for  $CuFe_2O_4$ ,  $28.69\%$  to  $38.40\%$  for  $NiFe_2O_4$ ,  $36.68\%$  to  $47.21\%$  for  $CoFe_2O_4$ ; while the content of  $Fe_3O_4$  decreased from  $67.33\%$  to  $58.80\%$  for  $CuFe_2O_4$ ,  $57.22\%$  to  $37.50\%$  for  $NiFe_2O_4$ ,  $17.31\%$  to  $14.90\%$  for  $CoFe_2O_4$ , respectively. These results implied that the  $CoFe_2O_4$  was readily reduced to  $FeO$  in comparison to  $CuFe_2O_4$  and  $NiFe_2O_4$ . The presence of  $FeO$  in the reduced samples implied that the  $Fe_3O_4$  was further reduced, and more oxygen was provided by  $CoFe_2O_4$ . This may explain why a large amount of  $CoFe_2O_4$  remained in the reduced sample, while  $CoFe_2O_4$  has higher  $\alpha_c$  and  $\eta_{CO_2}$  in the fluidized bed tests compared with  $NiFe_2O_4$ . Additionally, the simulation results showed that the contents of  $FeO$  in the reduced sample of  $NiFe_2O_4$  and  $CuFe_2O_4$  were not negligible at high temperatures. In fact, the peak of  $FeO$  was not observed in the XRD patterns of the reduced sample of  $NiFe_2O_4$  and  $CuFe_2O_4$  (Fig. 6). This could be due to incomplete reactions of PS and metal ferrites; thus, the  $Fe_3O_4$  was not further reduced to  $FeO$ .

## 4. Conclusions

Reaction reactivity of  $MFe_2O_4$  ( $M = Cu, Ni \text{ and } Co$ ) with pine sawdust was investigated in TGA and fluidized bed reactor. The oxygen carriers were characterized by XRD, SEM and BET. Thermodynamic simulation was performed using software HSC Chemistry 6.0. The following conclusions can be made:

- (1) Both TGA and fluidized bed experiments revealed that the reactivity of  $MFe_2O_4$  ( $M = Cu, Ni \text{ and } Co$ ) in CLC using PS as fuel decreased in the following order:  $CuFe_2O_4 > CoFe_2O_4 > NiFe_2O_4$ , and  $CuFe_2O_4$  has a lower initial reaction temperature.
- (2) Both carbon conversion ( $\alpha_c$ ) and carbon capture efficiency ( $\eta_{CO_2}$ ) increased with increasing temperature. The maximum values of  $\alpha_c$  and  $\eta_{CO_2}$  were  $96.86\%$  and  $95.65\%$ ,  $95.45\%$  and  $94.25\%$ , and  $95.17\%$  and  $94.04\%$  for  $CuFe_2O_4$ ,  $CoFe_2O_4$ , and

NiFe<sub>2</sub>O<sub>4</sub>, respectively. NiFe<sub>2</sub>O<sub>4</sub> has a higher catalytic reactivity for tar cracking and reforming compared with CuFe<sub>2</sub>O<sub>4</sub> and CoFe<sub>2</sub>O<sub>4</sub>.

- (3) The XRD patterns show that NiFe<sub>2</sub>O<sub>4</sub> was mainly decomposed into Fe<sub>3</sub>O<sub>4</sub> and Ni; CuFe<sub>2</sub>O<sub>4</sub> was reduced to Cu, Fe<sub>3</sub>O<sub>4</sub> and CuFeO<sub>2</sub>; and the reduction products of CoFe<sub>2</sub>O<sub>4</sub> were Co, FeO and Fe<sub>3</sub>O<sub>4</sub>. These results were in agreement with the thermodynamic simulation. After five redox cycles, three metal ferrites can be fully regenerated.
- (4) Both CuFe<sub>2</sub>O<sub>4</sub> and CoFe<sub>2</sub>O<sub>4</sub> have high thermal stability and maintained higher  $\alpha_c$  and  $\eta_{CO_2}$  values after five redox cycles; while  $\alpha_c$  and  $\eta_{CO_2}$  decreased significantly when NiFe<sub>2</sub>O<sub>4</sub> was used due to the impact of the severe sintering. These results were confirmed by BET and SEM. Thus, CuFe<sub>2</sub>O<sub>4</sub> and CoFe<sub>2</sub>O<sub>4</sub> are more applicable as oxygen carriers in biomass CLC compared with NiFe<sub>2</sub>O<sub>4</sub>.

## Acknowledgments

The authors wish to acknowledge the financial support by the National Natural Science Foundation of China (No. 21676112), the China Postdoctoral Science Foundation (2015M580644, 2016M592339), the Ministry of Housing and Urban-Rural Development (No. 2016K4032), and Wuhan International Science and Technology Cooperation Project (No. 2016030409020221). Meanwhile, the authors would also like to thank the Analytical and Testing Center of Huazhong University of Science & Technology for carrying out the analyses of pine sawdust and oxygen carrier samples.

## References

- [1] D. Narita, Managing uncertainties: the making of the IPCC's Special Report on Carbon Dioxide Capture and Storage, *Public Underst. Sci.* 21 (2012) 84–100.
- [2] Y. Tan, W. Nookuea, H. Li, E. Thorin, J. Yan, Property impacts on Carbon Capture and Storage (CCS) processes: a review, *Energy Convers. Manage.* 118 (2016) 204–222.
- [3] M.B. Toftgaard, J. Brix, P.A. Jensen, P. Glarborg, A.D. Jensen, Oxy-fuel combustion of solid fuels, *Prog. Energy Combust.* 36 (2010) 581–625.
- [4] M.M. Hossain, H.I. de Lasa, Chemical-looping combustion (CLC) for inherent CO<sub>2</sub> separations—a review, *Chem. Eng. Sci.* 63 (2008) 4433–4451.
- [5] E. Johansson, T. Mattisson, A. Lyngfelt, H. Thunman, Combustion of syngas and natural gas in a 300 W chemical-looping combustor, *Chem. Eng. Res. Des.* 84 (2006) 819–827.
- [6] M. Tang, L. Xu, M. Fan, Progress in oxygen carrier development of methane-based chemical-looping reforming: a review, *Appl. Energy* 151 (2015) 143–156.
- [7] H.B. Huang, L. Aisyah, P.J. Ashman, Y.C. Leung, C.W. Kwong, Chemical looping combustion of biomass-derived syngas using ceria-supported oxygen carriers, *Bioresour. Technol.* 140 (2013) 385–391.
- [8] H.R. Kim, D. Wang, L. Zeng, S. Bayham, A. Tong, E. Chung, M.V. Kathe, S. Luo, O. McGivern, A. Wang, Coal direct chemical looping combustion process: design and operation of a 25-kWth sub-pilot unit, *Fuel* 108 (2013) 370–384.
- [9] H. Leion, T. Mattisson, A. Lyngfelt, The use of petroleum coke as fuel in chemical-looping combustion, *Fuel* 86 (2007) 1947–1958.
- [10] X. Niu, L. Shen, H. Gu, T. Song, J. Xiao, Sewage sludge combustion in a CLC process using nickel-based oxygen carrier, *Chem. Eng. J.* 260 (2015) 631–641.
- [11] T. Mendiara, A. Abad, L.F. de Diego, F. García-Labiano, P. Gayán, J. Adánez, Biomass combustion in a CLC system using an iron ore as an oxygen carrier, *Int. J. Greenhouse Gas Control* 19 (2013) 322–330.
- [12] M.F. Demirbas, M. Balat, H. Balat, Potential contribution of biomass to the sustainable energy development, *Energy Convers. Manage.* 50 (2009) 1746–1760.
- [13] N. Kobayashi, L. Fan, Biomass direct chemical looping process: a perspective, *Biomass Bioenergy* 35 (2011) 1252–1262.
- [14] Á. Jiménez Álvaro, I. López Paniagua, C. González Fernández, J. Rodríguez Martín, R. Nieto Carlier, Simulation of an integrated gasification combined cycle with chemical-looping combustion and carbon dioxide sequestration, *Energy Convers. Manage.* 104 (2015) 170–179.
- [15] C. Wang, J. Wang, M. Lei, H. Gao, Investigations on combustion and NO emission characteristics of coal and biomass blends, *Energy Fuels* 27 (2013) 6185–6190.
- [16] S.V. Vassilev, D. Baxter, L.K. Andersen, C.G. Vassileva, An overview of the chemical composition of biomass, *Fuel* 89 (2010) 913–933.
- [17] J. Adanez, A. Abad, F. García-Labiano, P. Gayan, L.F. de Diego, Progress in chemical-looping combustion and reforming technologies, *Prog. Energy Combust.* 38 (2012) 215–282.
- [18] X. Niu, L. Shen, S. Jiang, H. Gu, J. Xiao, Combustion performance of sewage sludge in chemical looping combustion with bimetallic Cu–Fe oxygen carrier, *Chem. Eng. J.* 294 (2016) 185–192.
- [19] B. Wang, R. Yan, H. Zhao, Y. Zheng, Z. Liu, C. Zheng, Investigation of chemical looping combustion of coal with CuFe<sub>2</sub>O<sub>4</sub> oxygen carrier, *Energy Fuels* 25 (2011) 3344–3354.
- [20] S. Bhavsar, G. Vesper, Bimetallic Fe–Ni oxygen carriers for chemical looping combustion, *Ind. Eng. Chem. Res.* 52 (2013) 15342–15352.
- [21] Y. Kuo, W. Hsu, P. Chiu, Y. Tseng, Y. Ku, Assessment of redox behavior of nickel ferrite as oxygen carriers for chemical looping process, *Ceram. Int.* 39 (2013) 5459–5465.
- [22] Z. Huang, F. He, Y. Feng, K. Zhao, A. Zheng, S. Chang, G. Wei, Z. Zhao, H. Li, Biomass char direct chemical looping gasification using NiO-modified iron ore as an oxygen carrier, *Energy Fuels* 28 (2013) 183–191.
- [23] B. Wang, C. Gao, W. Wang, F. Kong, C. Zheng, TGA-FTIR investigation of chemical looping combustion by coal with CoFe<sub>2</sub>O<sub>4</sub> combined oxygen carrier, *J. Anal. Appl. Pyrolysis* 105 (2014) 369–378.
- [24] A. Evdou, V. Zaspalis, L. Nalbandian, Ferrites as redox catalysts for chemical looping processes, *Fuel* 165 (2016) 367–378.
- [25] D.S. Mathew, R. Juang, An overview of the structure and magnetism of spinel ferrite nanoparticles and their synthesis in microemulsions, *Chem. Eng. J.* 129 (2007) 51–65.
- [26] A.M. Banerjee, M.R. Pai, S.S. Meena, A.K. Tripathi, S.R. Bharadwaj, Catalytic activities of cobalt, nickel and copper ferrosinels for sulfuric acid decomposition: the high temperature step in the sulfur based thermochemical water splitting cycles, *Int. J. Hydrogen Energy* 36 (2011) 4768–4780.
- [27] L.Q. Qwabe, H.B. Friedrich, S. Singh, Preferential oxidation of CO in a hydrogen rich feed stream using Co-Fe mixed metal oxide catalysts prepared from hydroxalite precursors, *J. Mol. Catal. A: Chem.* 404–405 (2015) 167–177.
- [28] N. Ballarini, F. Cavani, S. Passeri, L. Pesaresi, A.F. Lee, K. Wilson, Phenol methylation over nanoparticulate CoFe<sub>2</sub>O<sub>4</sub> inverse spinel catalysts: the effect of morphology on catalytic performance, *Appl. Catal. A: Gen.* 366 (2009) 184–192.
- [29] C. Luadthong, P. Khemthong, W. Nualpaeng, K. Faungnawakij, Copper ferrite spinel oxide catalysts for palm oil methanolysis, *Appl. Catal. A: Gen.* 525 (2016) 68–75.
- [30] S.H. Xiao, W.F. Jiang, L.Y. Li, X.J. Li, Low-temperature auto-combustion synthesis and magnetic properties of cobalt ferrite nanopowder, *Mater. Chem. Phys.* 106 (2007) 82–87.
- [31] J. Li, B. Xiao, R. Yan, X. Xu, Development of a supported tri-metallic catalyst and evaluation of the catalytic activity in biomass steam gasification, *Bioresour. Technol.* 100 (2009) 5295–5300.
- [32] S.R. Elliott, *Physics of Amorphous Materials*, 1983, Longman Group, Longman House, Burnt Mill, Harlow, Essex CM 20 2 JE, England, 1983.
- [33] K. Kang, C. Kim, W. Cho, K. Bae, S. Woo, C. Park, Reduction characteristics of CuFe<sub>2</sub>O<sub>4</sub> and Fe<sub>3</sub>O<sub>4</sub> by methane; CuFe<sub>2</sub>O<sub>4</sub> as an oxidant for two-step thermochemical methane reforming, *Int. J. Hydrogen Energy* 33 (2008) 4560–4568.
- [34] H. Shin, S. Choi, K. Jung, S. Han, Mechanism of M Ferrites (M = Cu and Ni) in the CO<sub>2</sub> decomposition reaction, *Chem. Mater.* 13 (2001) 1238–1242.
- [35] Y. Fan, R. Siritwardane, Novel new oxygen carriers for chemical looping combustion of solid fuels, *Energy Fuels* 28 (2014) 2248–2257.
- [36] A.E. Katkov, A.A. Lykasov, Spinel phase relations in the Fe<sub>3</sub>O<sub>4</sub>–CuFe<sub>2</sub>O<sub>4</sub> system, *Inorg. Mater.* 39 (2003) 171–174.
- [37] P. Lv, Z. Yuan, C. Wu, L. Ma, Y. Chen, N. Tsubaki, Bio-syngas production from biomass catalytic gasification, *Energy Convers. Manage.* 48 (2007) 1132–1139.
- [38] C.G. Ramankutty, S. Sugunan, Surface properties and catalytic activity of ferrosinels of nickel, cobalt and copper, prepared by soft chemical methods, *Appl. Catal. A Gen.* 218 (2001) 39–51.
- [39] J.P. Jacobs, A. Maltha, J.G.H. Reintjes, J. Drimal, V. Poncet, H.H. Brongersma, The surface of catalytically active spinels, *J. Catal.* 147 (1994) 294–300.
- [40] B. Wang, G. Xiao, X. Song, H. Zhao, C. Zheng, Chemical looping combustion of high-sulfur coal with NiFe<sub>2</sub>O<sub>4</sub>-combined oxygen carrier, *J. Therm. Anal. Calorim.* 118 (2014) 1593–1602.
- [41] E. Manova, T. Tsoncheva, C. Estournès, D. Paneva, K. Tenchev, I. Mitov, L. Petrov, Nanosized iron and iron-cobalt spinel oxides as catalysts for methanol decomposition, *Appl. Catal. A Gen.* 300 (2006) 170–180.
- [42] J. Bao, Z. Li, N. Cai, Interaction between iron-based oxygen carrier and four coal ashes during chemical looping combustion, *Appl. Energy* 115 (2014) 549–558.
- [43] H. Gu, L. Shen, Z. Zhong, Y. Zhou, W. Liu, X. Niu, H. Ge, S. Jiang, L. Wang, Interaction between biomass ash and iron ore oxygen carrier during chemical looping combustion, *Chem. Eng. J.* 277 (2015) 70–78.